

Lab on a Chip

Accepted Manuscript



This is an *Accepted Manuscript*, which has been through the Royal Society of Chemistry peer review process and has been accepted for publication.

Accepted Manuscripts are published online shortly after acceptance, before technical editing, formatting and proof reading. Using this free service, authors can make their results available to the community, in citable form, before we publish the edited article. We will replace this *Accepted Manuscript* with the edited and formatted *Advance Article* as soon as it is available.

You can find more information about *Accepted Manuscripts* in the [Information for Authors](#).

Please note that technical editing may introduce minor changes to the text and/or graphics, which may alter content. The journal's standard [Terms & Conditions](#) and the [Ethical guidelines](#) still apply. In no event shall the Royal Society of Chemistry be held responsible for any errors or omissions in this *Accepted Manuscript* or any consequences arising from the use of any information it contains.

ARTICLE

Open-access optical microcavities for lab-on-a-chip refractive index sensing

Cite this: DOI: 10.1039/x0xx00000x

A. A. P. Trichet^a, J. Foster^b, N. E. Omori^a, D. James^b, P. R. Dolan^a, G. M. Hughes^a, C. Vallance^b and J. M. Smith^a

Received 00th January 2012,

Accepted 00th January 2012

DOI: 10.1039/x0xx00000x

www.rsc.org/

Open-access optical microcavities provide a novel approach to label-free lab-on-a-chip optofluidic sensing. They offer direct access to a highly confined electromagnetic field, and yield a femtoliter detection volume. This article describes the characteristics of these devices for refractive index sensing. We show that most of the ambient noise can be removed from the refractive index data by simultaneous tracking of resonances across an array of cavities. A sensitivity of 3.5×10^{-4} RIU is demonstrated which corresponds to detecting the refractive index change caused by the presence of 500 000 glucose molecules in aqueous solution.

Introduction

Photon-based detection schemes for lab-on-a-chip sensors offer the potential for flexible and non-destructive measurement of on-chip chemical species¹⁻⁴. Many photonic devices are now miniaturised down to the micron scale, making them highly compatible with the size, power, and portability requirements of microfluidic sensors. Detection methods employing optical cavities offer particular promise for lab-on-a-chip applications, since the intrinsic multi-pass nature of such methods overcomes the very short optical path length accessible within a microfluidic channel⁵. Various authors have demonstrated a sensitivity enhancement of one to two orders of magnitude for optical absorption measurements using a variety of cavity-enhanced absorption methods⁶⁻⁹. The achievable detection sensitivity in most of these approaches is limited by the fact that a microfluidic chip or flow cell is inserted into the optical cavity, leading to reflection and scattering losses at the additional surfaces introduced into the cavity.

Microcavities or microresonators, such as photonic crystals¹⁰⁻¹¹, ring resonators¹²⁻¹³ and plasmons resonators¹⁴⁻¹⁵, have also attracted much attention in recent years as a result of their performance in chemical sensing applications. The resonant frequencies of light that can circulate in such microresonators are exquisitely sensitive to changes in refractive index at the resonator surface, and tracking the mode frequencies therefore allows changes in refractive index to be detected. Moreover, chemical functionalization of the resonator surface allows the detection to be made species-selective by detecting the refractive index change caused by binding of the

selected target molecule. Detection limits down to the single molecule level have been reported using such approaches^{1-4,14,15}.

While optical microresonators of the type described above offer spectacular detection sensitivities with selectivity, they are intrinsically surface-sensitive detectors. Therefore, they are not well-suited to applications requiring detection across an entire microfluidic channel, such as, for example, direct monitoring of chemical reaction dynamics. In this respect, bulk sensors, such as hollow waveguides¹⁶, offer an alternative solution. In the present article, we present a new approach to miniaturized bulk refractive index sensors using arrays of open-access optical microcavities. In this configuration, the sample is contained in between plano-concave mirrors. Consequently, our method intrinsically provides a volume-sensitive detection scheme down to tens of femtoliters that can be naturally coupled to microfluidics channels in the future.

We report here the first results demonstrating refractive index sensing of glucose in open-access cavities, with a measured limit of 3.5×10^{-4} RIU. The very small liquid volumes probed within our device (around 50 fL) mean that the method is sensitive to the presence of around 5×10^5 molecules, or 900 zeptomoles of glucose. By employing a detection scheme involving simultaneous monitoring of several cavities, we are able to eliminate noise arising from variations in the cavity length, thus removing the need for active stabilization or isolation of the device and simplifying the experimental setup considerably. Optical microcavities offer a number of possible approaches to chemical sensing, and the work reported in the present article represents the first demonstration of this new category of chemical sensors. In future work, we will demonstrate how alternative detection schemes allow species-specific detection to be achieved. However, at present the detection method is universal and offers no selectivity for particular chemical species.

Experimental setup

Open-access microcavities are made up of two separate mirrors facing each other and which can move independently. The plano-concave mirror configuration employed in our device is shown in Figure 1(a). The microcavities are constructed from two separate substrates: an array of concave micromirrors and a planar mirror positioned a few microns apart. To undergo constructive interference

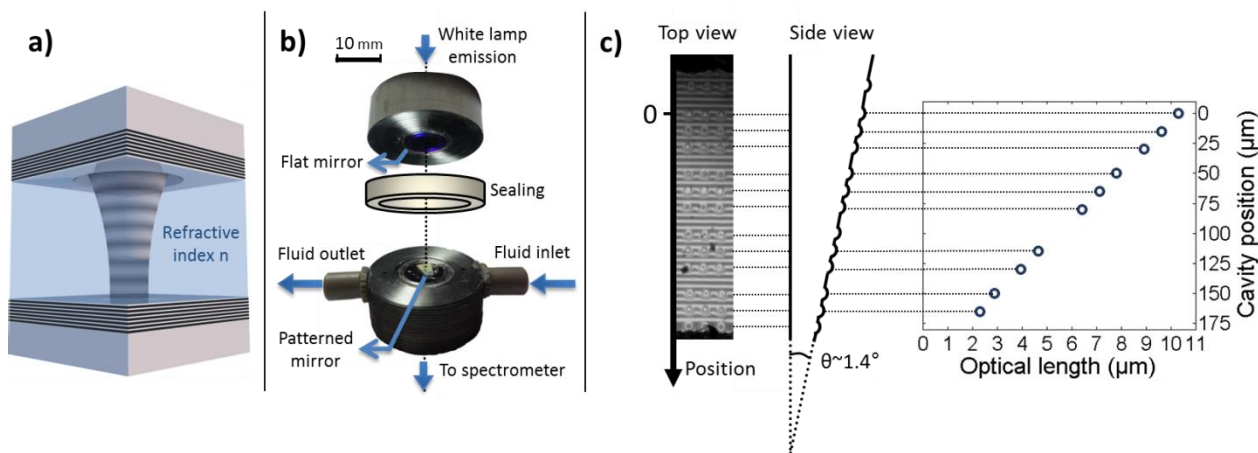


Figure 1: a) Schematic representation of an open-access cavity, with the planar surface at the base and the concave surface at the top; b) Exploded view of the flow cell. The flat mirror and the patterned mirrors are, respectively, at the top and bottom of the flow cell. The white lamp emission is focused on the flat mirror, then go through the patterned one before being sent to the spectrometer; c) Top view (photo) and side view (scheme) of the wedged mirrors (tilt-angle $\approx 2.8^\circ$). In the top view, the sample is illuminated by a 532nm (+/- 1nm) light. The observed fringes result from the variation in cavity length in the vertical direction. The cavities are arranged in 3x3 arrays. For the experiment discussed in this paper, only the middle column has been selected, corresponding to four sets of three cavities in a 12 x 1 array. The graphic on the right demonstrates the linear relationship between the optical length of each cavity with its position in the array. Two cavities in the array did not show transmission peaks and have been discarded.

between the mirrors, and therefore be confined within the cavity, a half integer number of wavelengths must match the cavity length, leading to the condition:

$$\frac{q\lambda}{2n} = L \quad (1)$$

for light propagating along the cavity axis, where λ is the wavelength, n is the refractive index of the medium within the cavity, and L is the cavity length. The resonant wavelengths are known as *longitudinal cavity modes*, and are characterised by their mode number, q . The concave mirrors result in transverse confinement of the light. Excitation of a given longitudinal mode along the mirror plane gives rise to a family of *transverse modes*. For a typical microcavity with a mirror separation of a few microns, the free spectral range (frequency spacing between longitudinal cavity modes) is so large that only a few wavelengths are resonant within the cavity. From Equation (1), it can be seen that a change in refractive index of the medium within the cavity (see Figure 1 (a)) leads to a shift in the resonant wavelengths, providing a means of monitoring the refractive index of a liquid flowing between the cavity mirrors. As we shall show, the micron-scale cavity length yields large shifts in resonance frequency in response to refractive index changes, offering highly sensitive label-free detection.

Based on our previous work¹⁷, the required small radius of curvature mirror substrates with high surface quality were fabricated by focused ion beam (FIB) milling (using a FEI FIB200) of fused silica plates (UQG Optics). The smallest lateral features that may be fabricated using this technique are limited by the size of the ion beam focus to around 5 nm, while the RMS surface roughness is found to be below 1 nm, close to the atomic resolution of the material. 3 x 3 arrays of micromirror substrates were fabricated, with each mirror having a diameter of 10 μm and a nominal radius of curvature, R , of 25 μm, similarly to our previous work in reference 17. The microfabricated and planar substrates were then coated in-house with dielectric mirrors comprising ten layers of SiO₂/TiO₂ ($n = 1.4$ and 2.1) with layer thicknesses tuned to achieve maximum reflectivity around 99.7% at 640 nm. Due to the low densities of the films, their refractive indices are slightly lower than those of bulk SiO₂ and TiO₂. In our case the primary limitation on the finesse is

the reflectivity of the dielectric coating. Indeed, the scattering-limited cavity finesse by the measured RMS roughness is above 10⁴ while the cavity finesse has been measured to be on the order of hundreds to one thousand depending on the cavity length for an empty cavity which is in agreement with the maximum finesse expected for our dielectric Bragg mirrors (around 10³). The quality factor is simply given by the finesse times the longitudinal mode number.

Once the mirrors are mounted into a custom-made flow cell (see exploded view in Figure 1 (b)), the top and bottom mirrors are brought close to each other and compress a silicone rubber sealing to create a microfluidic channel between the mirrors. In this way the entire cavity arrays are immersed in liquid. Fluid is flowed into and out of the flow cell and cavities through a pair of nanoports mounted on the bottom part of the flow cell. For the experiments described here, the flow cell was initially filled with deionised water. The wavelength shifts were measured on replacing the deionised water with an aqueous solution of glucose at a concentration of 1.390M +/- 0.002M. All liquids were pumped through the flow cell using a Fusion 400 syringe pump at a flow rate of 0.3 mL.min⁻¹.

To record the spectrum of cavity modes, the cavities are illuminated by a white light from a quartz halogen lamp (Bentham WLS100). Light transmitted through the cavities is focused into an Andor combined spectrograph/CCD with a 300 grooves per mm grating, which records cavity spectra every 100 ms. Using the multi-track feature of the spectrograph, spectra may be recorded simultaneously for 10 cavities at 100 ms intervals (see Figure 1(c)) as liquid samples were introduced into the flow cell (see Figure 2 (a)). In parallel with recording the cavity spectra, a second video camera monitored the flow cell to allow potential interference from air bubbles, dust, or vibrations to be identified.

In order to allow discrimination between a change in refractive index of the flow cell contents and a change in cavity length, as described in the next Section, the cavities are mounted in a wedged configuration, in which one mirror surface is tilted at an angle of 2.8 degrees with respect to the other, such that each cavity in the array has a slightly different length. This is demonstrated in the interferogram shown in Figure 1(b). The cavity modes are not

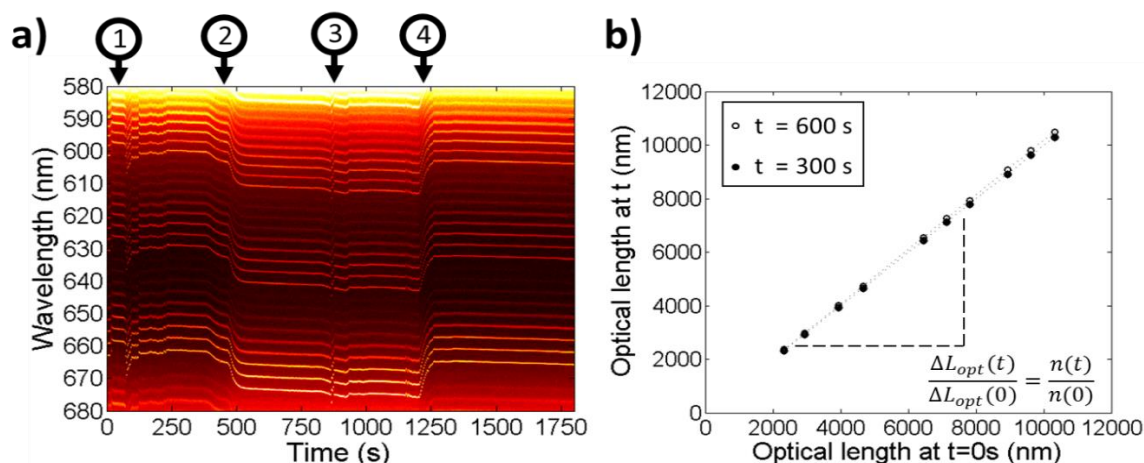


Figure 2: a) White lamp transmission of a single cavity recorded as a function of time. The times at which different steps in the experimental protocol occur are marked by numbers above the spectra. Initially, the cavity contains deionised water. At (1), a syringe containing glucose solution is connected to the syringe pump and the solution is flowed into the flow cell. At (2), the glucose solution reaches the cavity and causes a shift in the resonant wavelengths. At (3), the glucose-filled syringe is replaced with a syringe containing deionised water, and this is flowed through the system. At (4), the deionised water reaches the cavity, and the resonant frequencies return to their original values. b) Optical path length at time t vs optical path length at time $t = 0$ s for different cavities. Plots are shown for two different times, $t = 300$ s and $t = 600$ s, ie. just before and after the resonance shift (2), . The small difference in the slope reflects the change in refractive index.

significantly affected by the introduction of the small tilt angle between the mirrors, and while the physical distance between the mirrors is difficult to measure accurately, the *optical* path length through the cavity, discussed further in the next section, is straightforward to measure via the measured free spectral range of each cavity. The optical path length varies from $2.238 \mu\text{m}$ to $10.318 \mu\text{m}$ across the array of cavities, which spans a width of $165 \mu\text{m}$ within the flow cell.

Refractive index extraction method

By recording data from multiple cavities with different lengths it becomes possible to separate the shift in resonant wavelength arising from a change in refractive index from that induced by a change in cavity length. Small changes in cavity length over the course of an experiment as a result of vibrations, pressure change or thermal fluctuations are difficult to avoid, and it is important to be able to distinguish their effects from those of the refractive index changes to be measured. We first illustrate the problem by considering the resonant modes of a single cavity.

A plano-concave cavity sustains Hermite-Gaussian cavity modes when the mirror spacing or geometric length of the cavity, L_{geo} , is smaller than the radius of curvature R of the concave mirror. The optical path length L_{opt} within the cavity depends on the mirror spacing, the refractive index n of the medium within the cavity, and also on the penetration depth L_{DBR} into the dielectric Bragg reflecting mirror coatings, ie.:

$$L_{opt} = nL_{geo} + 2L_{DBR} \quad (2)$$

Generalising Equation (1) to take account of both penetration into the mirror surfaces and the potential presence of both longitudinal and transverse cavity modes, the resonant wavelengths for the cavity modes are given by:

$$\left[q + \frac{1}{\pi}(l + m + 1) \arccos \left(\sqrt{1 - \frac{L_{geo}}{R}} \right) \right] \frac{\lambda}{2} = nL_{geo} + 2L_{DBR} \quad (3)$$

where q is the longitudinal mode number and l and m are the transverse mode numbers. Assuming that L_{geo} varies by no more than a few tens of nanometers over the course of a measurement, the term involving L_{geo} can be treated as constant to within around one part in 10^6 , and the left hand side of Equation (3) simplifies to $\frac{q'\lambda}{2}$, where q' is a constant for a given mode but is no longer an integer. The shift in resonance wavelength arising from a variation in the refractive index and/or the cavity length, may then be written

$$\frac{\Delta\lambda}{\lambda} = \frac{nL_{geo}}{L_{opt}} \left(\frac{\Delta L_{geo}}{L_{geo}} + \frac{\Delta n}{n} \right) \quad (4)$$

We see that for a single cavity, one cannot discriminate between the effect of a refractive index change and the effect of a mirror displacement on the wavelengths of the resonant modes.

By using multiple cavities instead of a single cavity, the problem can be resolved, provided that each cavity suffers the same mirror displacements as a function of time. In our experimental setup, all of the concave mirrors are patterned onto a single substrate making this an excellent approximation in our case. However, this method cannot remove the ambient noise inducing a change in the tilt-angle in between the mirrors. Nevertheless, any angle drift will result in a constant drift on the refractive index. The stability of the refractive index that we observe as an output of our method is therefore an excellent indication that most of our cavity length noise is caused by a displacement rather than an angle. In the following, we assume that each cavity suffers an identical time-dependent mirror displacement noise $\delta L(t) = L_{geo}(t) - L_{geo}(0)$. Allowing for both n and L_{geo} to be time dependent in Equation (2), substituting $\delta L(t)$ as defined above, with $L_{geo}(0)$ as defined in Equation (2), yields:

$$q^i \frac{\lambda^i(t)}{2} = \left[\frac{n(t)}{n(t=0)} \right] L_{opt}^i(t=0) + \left[n(t)\delta l(t) + 2L_{DBR} \left(1 - \frac{n(t)}{n(t=0)} \right) \right] \quad (5)$$

where the index i identifies a particular cavity in the array. We see that only the first term on the right hand side of Equation (5) changes from cavity to cavity, and also that there is a linear relationship between the optical path length $q^i \lambda^i(t)/2 = L_{opt}^i(t)$ at time t , and the optical path length $L_{opt}^i(t \neq 0)$ at time 0 (see Figure

2 (b) for the experimental data). Plotting these two quantities against each other for each cavity in the array yields a slope $n(t)/n(0)$, allowing changes in refractive index to be tracked as a function of time. Equation (5) therefore represents the key result that allows us to measure small changes in refractive index. Note that the parameter $q'(i)$ can be measured for each cavity at $t = 0$, and remains constant so long as the same cavity mode is tracked with time.

If we assume that any change $\delta L(t)$ in the cavity lengths is much smaller than any of the other length parameters, Equation (5) can be rearranged and used to determine the penetration depth L_{DBR} into the mirrors.

$$L_{\text{DBR}} = \frac{q' i \frac{\lambda^i(t)}{2} - \left[\frac{n(t)}{n(t=0)} \right] L_{\text{opt}}^i(t=0)}{2 \left(1 - \frac{n(t)}{n(t=0)} \right)} \quad (6)$$

Using the data set discussed in the next section, we have determined the penetration depth L_{DBR} to be (570 ± 20) nm. Based on reference 18, the theoretical value for the penetration depth is 520 nm, in reasonably good agreement with our measurement.

Results

A sample set of time-dependent spectra recorded over 30 minutes for a single cavity while the flow cell was flushed first with deionized water, then with a 1.390M \pm 0.002M solution of glucose, then again with deionized water is shown in Figure 2(a). The cavity mirrors are reflective over a wavelength range spanning approximately 590 to 680 nm. Outside this range light of any wavelength is transmitted directly through the cavity. A vertical cut through the data in Figure 2 (a) at a given time yields a cavity spectrum consisting of a series of peaks corresponding to three families of longitudinal modes, each of them have a different longitudinal mode number q . For each longitudinal mode, there is a family of transverse modes (ie. $l, m \neq 0$). During the data analysis process, we focus only on pure longitudinal modes, since they do not have complex spectral mode structure, and are therefore easily fitted. The free spectral range between two consecutive longitudinal modes provides a direct measurement of the optical path length through the cavity. When carrying out the fitting procedure developed in the previous section to determine $n(t)/n(0)$, we fit only modes at wavelengths close to the 640 nm design wavelength of the mirror coatings, since these have the narrowest linewidth. In Figure 2 (a), four important events are labelled: (1) Plugging-in and mounting of a syringe of glucose solution into the syringe pump and commencement of pumping of the solution through the flow cell (2) Resonance red-shift due to the refractive index increase upon introduction of glucose into the cavity (3) Mounting of a syringe filled with deionised water in the syringe pump, and commencement of pumping (4) Resonance blue-shift as the water flushes the glucose from the cavity and the refractive index decreases back to its original value. The effect of the refractive index is directly observed for events (2) and (4). However, some extra noise is observed at different time (for example before (2) and (4)) and there is a persistent drift of the mode wavelengths with time. These noise events come from vibrations in the room, fluid pressure changes, spring relaxation or thermal expansion of materials via temperature changes.

Figure 2(b) shows the plot of the measured optical path lengths of ten different cavities at two different times, $t_1 = 300$ s and $t_2 = 600$ s, against their corresponding optical path lengths at $t = 0$ s. Recall that the glucose solution enters the cavities at $t \approx 500$ s, so the slopes of the two plots correspond to values of $n(t)/n(0)$. The result of performing this analysis to track the refractive index at every recorded time between $t = 300$ s and $t = 800$ s is shown in black line

on Figure 3 (b). Initially, while the cell is filled with deionized water, the refractive index is constant and shows no drift, demonstrating the reliability of the method we have developed. The same is true at later times, once the microcavity array is filled with glucose solution. For comparison, the grey line in Figure 3 (b) corresponds to the refractive index measurement from a single cavity assuming it is not affected by the length noise. In addition to a constant drift, it shows spikes and random fluctuations which are completely removed on the corrected measurement. The refractive index shows a rather complicated time dependence as the glucose solution enters the microcavity array, with the transition occurring over a period of around 100 s. This transient behaviour is a result of the flow cell geometry which leads to a combination of flow and diffusion. According to flow rate dependent experiments (not shown), the surrounding of the mirrors is mainly flow driven while the penetration of the analyte in between the mirrors is mainly diffusion driven. This is in agreement with the sizes of the flow cell pieces separation (≈ 0.5 mm) and the mirrors spacing ($\approx \mu\text{m}$).

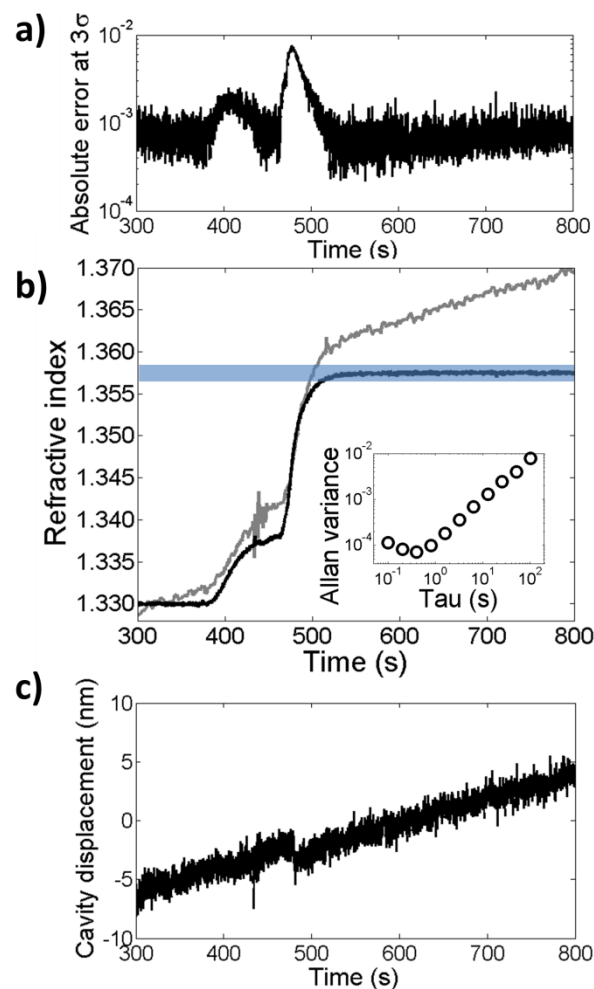


Figure 3: a) Absolute error (logscale) of the measured refractive index (confidence interval: 3σ); b) Black line: measured refractive index. The blue region is the expected refractive index from the glucose solution. Grey line: Refractive index measurement assuming no cavity length noise using a single cavity (from the spectrum of the cavity with the smallest length). Inset: Allan variance for the measured refractive index as a function of the sampling time; c) Cavity displacement as a function of time associated to the refractive index measurement in b).

Tracking the refractive index during the transition period should in principle allow the diffusion coefficient of the glucose molecule to be determined but in practice this is not easily achievable at present.

The 3σ uncertainty in the refractive index measured with a spectrometer sampling time of 100 ms is plotted in Figure 3(a), and provides a good indication of the limit of detection. In the regions of the plot corresponding to deionized water and glucose solutions, the uncertainty is 7×10^{-4} RIU. The minimum in an Allan variance plot can be used to determine the optimum sampling time under the conditions of our experiment. The optimum sampling time represents a balance between increasing the number of data points that are averaged, in order to reduce the noise, and not averaging significantly over any true time dependence in the signal. The Allan variance plot shown in the inset to Figure 3(b) indicates that for the signal shown in the main plot, the optimal sampling time is 400 ms. Re-averaging the data over this time reduces the 3σ limit of detection to 3.5×10^{-4} RIU.

During the resonance shift, while the glucose solution is diffusing into the cavity, the uncertainty in the refractive index is seen to be much higher, with the values in the plot shown in Figure 3(a) increasing by up to a factor of ten. This increased uncertainty arises because the glucose solution fills the microcavities in the array one by one, so there is a delay in the wavelength shift recorded from cavity to cavity. For example, the wavelength shift in the final cavity to be filled is delayed by around 8 seconds compared with that measured of the first cavity to be filled. Improving the flow dynamics of the cell would mitigate these effects considerably. Notice that the peak at 434 seconds on the refractive index measurement on Figure 3 (b) is within the 3σ error given by Figure 3 (a) at the same time, ie. the absolute error is 1.8×10^{-3} .

Using the time-dependent refractive index plotted in Figure 3(b) together with the mirror penetration depth L_{DBR} determined in the previous section, we can use Equation (5) to determine the time-dependent mirror displacement $\delta L(t)$. This is plotted in Figure 3(c) for the longest cavity, and is found to be the same for all cavities (within an uncertainty of 1 nm). The cavity lengths are seen to undergo a constant drift of around 10 nm with time. An additional ~ 1 nm shift is seen at $t = 480$ s, the origin of which is unknown. However, no corresponding feature is seen in the refractive index plot shown in Figure 3 (b), providing further support for the robustness of the data analysis procedure.

While there are many approaches to refractive index sensing with sensitivity better than the 3.5×10^{-4} RIU achieved here, there are very few, if any, capable of detecting refractive index changes of this magnitude in the tiny volumes of liquid probed in the present experiments. The detection volume, V_d , is simply the sum of the mode volumes of the cavities in the array, given by

$$V_d = \sum_i \frac{\pi(\omega_0^i)^2 L_{\text{geo}}^i}{4n} \quad (7)$$

where ω_0^i is the mode waist on the flat mirror for the i^{th} cavity for $n = 1$. The total volume of detection in our experimental setup is $54 \mu\text{m}^3$, or 54 femtolitres. Therefore, we calculate that at our limit of detection we can detect the modification of refractive index resulting from the introduction of 500 000 molecules (900 zeptomoles) of glucose into the device. The limit of detection reported here is not intrinsic, and is limited by the accuracy of the fit to each mode peak. Improved sensitivity can therefore be achieved by increasing the intensity of the light source, the sensitivity of the detector, the resolution of the spectrograph, or the finesse of the cavities. In the future, we should improve the cavity finesse by two orders of magnitude, while further reducing the mode volume.

Conclusion

We have presented a new method for refractive index sensing using open-access microcavities. Our sensitivity of 3.5×10^{-4} RIU in a 54 fL detection volume corresponds to the detection of 5×10^5 glucose molecules. By recording data simultaneously from multiple cavities, we have shown that shifts in the resonant cavity modes caused by refractive index changes and physical mirror displacements can be decoupled, thereby overcoming an inherent challenge for sensors based on open-access cavities.

Open-access microcavities are a promising technology for lab-on-a-chip applications. Improved specifications have potential to move the approach into the realm of single molecule detection, and by exploiting further features of optical microcavities it may even be possible to carry out independent measurements of molecular sizes and polarisabilities at the single molecule level, representing a major breakthrough in the field of optical sensing.

Acknowledgements

This work was funded by the Royal Society and the Leverhulme Trust.

Notes and references

^a Department of Materials, University of Oxford, OX1 3PH, UK

^b Department of Chemistry, University of Oxford, OX1 3QR, UK

- 1 F. Vollmer, L. Yang, *Nanophotonics*, 2012, **1**, 267-291
- 2 C. Monat, P. Domachuk, B. J. Eggleton, *Nature Photonics*, 2007, **1**, 106-114
- 3 T. Yoshie, L. Tang, S. Su, *Sensors*, 2011, **11**, 1972-1991;
- 4 H. K. Hunt, A. M. Armani, *Nanoscale*, 2010, **2**, 1544-1559;
- 5 C. M. Rushworth, J. Davies, J. T. Cabral, P. R. Dolan, J. M. Smith, and C. Vallance, *Chem. Phys. Lett.*, 2013, **554**, 1-14;
- 6 S. C. Xu, G. H. Sha, J. C. Xie, *Rev. Sci. Instrum.*, 2002, **73(2)**, 255-258;
- 7 B. Bahnev, L. van der Sneppen, A. Wiskerke, F. Ariese, C. Gooijer, W. Ubachs, *Anal. Chem.*, 2005, **77**, 1188-1191;
- 8 D. James, B. Oag, C. M. Rushworth, J. W. L. Lee, J. Davies, J. T. Cabral, C. Vallance, *RSC Advances* 2, 2012, 5376-5384;
- 9 A. Nitkowski, L. Chen, M. Lipson, *Optics Express*, 2008, 16 (16), 11930-11936
- 10 D. Dorfner, T. Zabel, T. Hürlimann, N. Hauke, L. Frandsen, U. Rant, G. Abstreiter, J. Finley, *Biosensors and Bioelectronics*, 2009, 24, 3688-3692
- 11 Y. Liu, H. W. M. Salemink, *Optics Express*, 2012, **20 (18)**, 19912-19920
- 12 I. M. White, H. Zhu, J. D. Suter, N. M. Hanumegowda, H. Oveys, M. Zurob, X. Fan, *IEEE Sensors Journal*, 2007, **7**, 28-35
- 13 Y. Sun, X. Fan, *Anal. Bioanal. Chem.*, 2011, **399**, 205-211
- 14 P. Zijlstra, P. M. R. Paulo, M. Orrit, *Nature Nanotechnology*, 2012, **7**, 379-382;
- 15 J. N. Anker, W. P. Hall, O. Lyandres, N. C. Shah, J. Zhao, R. P. Van Duyne, *Nature Materials*, 2008, **7**, 442-453
- 16 S. Campopiano, R. Bernini, L. Zeni, P. M. Sarro, *Optics Letters*, 2004, **29 (16)**, 1894-1896
- 17 P. R. Dolan, G. M. Hughes, F. Grazioso, B. R. Patton, J. M. Smith, *Optics letters*, 2010, **35 (21)**, 3556-3558;
- 18 L. R. Brovelli, U. Keller, *Optics Communications*, 1995, **116**, 343-350